



# CHORUS

This is the accepted manuscript made available via CHORUS. The article has been published as:

## Role of dissolved salts in thermophoresis of DNA: Lattice-Boltzmann-based simulations

Audrey Hammack, Yeng-Long Chen, and Jennifer Kreft Pearce

Phys. Rev. E **83**, 031915 — Published 24 March 2011

DOI: [10.1103/PhysRevE.83.031915](https://doi.org/10.1103/PhysRevE.83.031915)

# Role of dissolved salts in thermophoresis of DNA: Lattice Boltzmann based simulations

Audrey Hammack,<sup>1</sup> Yeng-Long Chen,<sup>2,3</sup> and Jennifer Kreft Pearce<sup>1,\*</sup>

<sup>1</sup>*Department of Chemistry, University of Texas at Tyler, Tyler, TX*

<sup>2</sup>*Institute of Physics, Academia Sinica, Taipei, Taiwan*

<sup>3</sup>*Research Center for Applied Science, Academia Sinica, Taipei, Taiwan*

We use a lattice Boltzmann based Brownian dynamics simulation to investigate the dependence of DNA thermophoresis on its interaction with dissolved salts. We find the thermal diffusion coefficient  $D_T$  depends on the molecule size, in contrast with previous simulations without electrostatics. The measured  $S_T$  also depends on the Debye length. This suggests thermophoresis of DNA is influenced by the electrostatic interactions between the polymer beads and the salt ions. However, when electrostatic forces are weak, DNA thermophoresis is not found, suggesting that other repulsive forces such as the excluded volume force prevent thermal migration.

PACS numbers: 87.14Gk, 82.35Rs, 66.10cd

## I. INTRODUCTION

Thermophoresis, also known as thermal diffusion or the Soret effect, is the migration of a species due to a temperature gradient. Understanding the phenomenon has proved challenging since results from different experiments often contradict each other because of the complexity of the underlying mechanism [1–9]. Particle thermophoresis can be obscured by particle transport by thermal convection, and thermophoresis in multi-component mixtures is further complicated by the interaction between different species. In particular, thermophoresis of charged particles is complicated by the thermal migration of salt ions, which induces an electric field when the cations and anions have very different thermodiffusivities [8, 9]. When the induced electric field is strong, the particle thermodiffusivity has been found to be directly proportional to the field strength. When the field is weak, particle thermodiffusion is found to be quenched at high ionic strengths. This study will focus on the role played by interspecies interactions on particle thermodiffusion in a binary mixture, and neglect the effects of fluid thermal convection.

To quantify results, the flux of a migrating species is described by Ficks Law, with an extra term to account for thermal diffusion:

$$J_y = -\rho \frac{\partial B}{\partial y} D - \rho D_T B(1 - B) \frac{\partial T}{\partial y} \quad (1)$$

where  $J_y$  is the particle flux in the  $y$ -direction. The first term denotes diffusion due to a concentration gradient:  $D$  is the molecular diffusion coefficient,  $B$  is the concentration of the migrating species and  $\rho$  is the mass fraction. The second term describes diffusion due to the temperature gradient:  $D_T$  is the thermal diffusion coefficient and  $T$  is the local temperature. A third term can

be added to the equation to account for electrophoresis if an electric field is present. At steady state,  $J_y=0$  and the Soret coefficient,  $S_T$  is defined as

$$S_T = \frac{D_T}{D} = \frac{-1}{B(1 - B)} \frac{\partial B / \partial y}{\partial T / \partial y} \quad (2)$$

$S_T$  can be positive or negative depending on whether the species migrates to the hot ( $S_T < 0$ ) or the cold ( $S_T > 0$ ) region. In fact, the sign of  $S_T$  has been shown to change in experiments depending on the physical parameters of the system[10–13].

As examples of the difficulties in understanding this phenomena, we summarize the results found in [1–6, 8, 9, 13]. It is common for different experiments on the same migrating species to observe different determining factors for the value of  $S_T$  and  $D_T$ . In [9, 13], the mechanism of thermophoresis of sodium dodecyl sulfate (SDS) micelles or nanoscale latex spheres in solution depended on the type of salt also dissolved in the solution. Two different scenarios were observed: if the cation and anion have significantly different  $S_T$  values, an electric field would develop akin to the Seebeck effect in solids due to differences in thermal migration of the ions. If the salt did not differentially migrate, electrokinetics did not play a significant role in determining migration of the larger species.

Similarly, two regimes for the thermophoretic mobility for polymers have been reported [3, 4]. In the dilute polymer regime, the bulk solvent viscosity determines  $D_T$ . Near the polymer glass transition, the effective local polymer viscosity determines the thermophoretic mobility. In addition,  $D_T$  for neutral polymers has been shown to be molecular weight independent [2].  $D_T$  for charged polymers, in contrast, has been measured to increase with decreasing molecular weight [1, 6].

Additionally, observations in [6] found that  $D_T$  varied with particle size in colloidal suspensions, while the work of Piazza et al. [8] did not find the same size dependence. The particle composition in both studies was similar, but particle surface treatments were used in [8] to standardize interfacial properties. Finally, in the work of Duhr

\*Corresponding author: jkref@uttyler.edu

et al. [5],  $D_T$  for double stranded DNA remained constant for the two different lengths examined (48.5 kbp and 27 bp), with  $D_T = 0.4\mu\text{m}^2/\text{s}/K$ . However, Duhr and Braun later found that  $D_T$  decreases with increasing DNA length [6]. The difference between these two experiments could be due to the lower salt concentration and stronger electrostatic forces in the later work. We will test this hypothesis by measuring the thermal diffusion coefficient and Soret coefficient for DNA in a simulation which allows direct observation of the DNA-ion interactions.

Several models based on both local equilibrium [6, 14, 15] and non-equilibrium [16–22] assumptions have been developed to interpret these complex experimental results. Dhont et al., proposed a model based on force balance for the thermal diffusion coefficient of charged colloidal particles [14]. In the limit of thin electric double layers, this model is equivalent to those proposed by Fayolle, *et al.* and Duhr and Braun [6, 15]. This theory does match some experiments [6, 23], but not others [8, 9]. Studies indicate that thermophoresis of charged micelles and nanoscale latex spheres are strongly influenced by an electric field that develops as positive ions migrate differently than negative ions in solution. This leads to a slight charge accumulation at the boundaries of the container and an electric field that influences the motion of the micelles [9, 13]. Würger proposed a model based on the development of an electrolyte-induced electric field for spherical particles much larger than the Debye length that captures the qualitative trends observed in [9]. Others have proposed models for thermophoresis that are based on a non-equilibrium approach that nearly quantitatively match experiments [16–21]. Of these approaches, either based on equilibrium or non-equilibrium thermodynamics, no single model satisfactorily captures all reported trends. Under different experimental conditions, different interactions may dominate thermophoretic mobility; both equilibrium and non-equilibrium approaches are needed to fully capture the thermophoresis mechanism.

To shed light on the differences between the two recent experiments on DNA thermophoresis [5, 6], we present data from a simulation that employs the lattice Boltzmann model for hydrodynamics and a worm-like chain model with Brownian dynamics for the DNA. The model allows us to capture the long time scales needed for the experimental system to equilibrate in a relatively short amount of computing time [24, 25]. The role and dynamics of dissolved ions on DNA thermophoresis cannot be easily measured in experiment. However, the simulation is able to capture and quantify the motions of DNA chains, salt ions, and counterions.

## II. SIMULATION

### A. Fluid Model

The simulation employs the lattice Boltzmann method (LBM) to solve for the velocity distribution of solvent molecules on fixed lattice sites at each time step [26–30]. We use this model as it is an explicit model for fluid-particle and fluid mediated particle-particle interactions, rather than implicit, as in some Brownian dynamics simulations [25]. The forces in the simulation include hydrodynamic interactions between particles. The fluid-particle interaction is necessary to reproduce thermophoresis [24]. The fundamental quantity in the LBM is  $n_i(\mathbf{r}, t)$ , which describes the distribution of solvent molecules with a discretized velocity,  $\mathbf{c}_i$  at position  $\mathbf{r}$  and time  $t$  [28]. The maximum velocity in the simulation is the speed of sound,  $c_s = \sqrt{1/3}\Delta x/\Delta\tau$ , where  $\Delta x = 1$  is the lattice spacing in simulation units and  $\Delta\tau = 0.05$  is the fluid timestep in simulation units ( $\Delta x = 0.5\mu\text{m}$  and  $\Delta\tau = 8.8 \times 10^{-6}\text{s}$ ). At equilibrium, the velocity distribution of solvent molecules will be Maxwell-Boltzmann, and can be represented by a second-order expansion:

$$n_i^{eq} = \rho a^{c_i} [1 + (\mathbf{c}_i \cdot \mathbf{u})/c_s^2 + \mathbf{u}\mathbf{u} : (\mathbf{c}_i\mathbf{c}_i - c_s^2\mathbf{I})/(2c_s^4)] \quad (3)$$

where  $\rho$  is the density,  $\mathbf{u}$  is the local velocity, and  $\mathbf{I}$  is the identity matrix. The coefficients  $a^{c_i}$  are found by satisfying the local isotropy condition:

$$\sum a^{c_i} \mathbf{c}_{i\alpha} \mathbf{c}_{i\beta} \mathbf{c}_{i\gamma} \mathbf{c}_{i\delta} = c_s^4 (\delta_{\alpha\beta} \delta_{\gamma\delta} + \delta_{\alpha\gamma} \delta_{\beta\delta} + \delta_{\alpha\delta} \delta_{\beta\gamma}) \quad (4)$$

where  $\alpha$ ,  $\beta$ ,  $\delta$ , and  $\gamma$  represent the x, y, or z axis. The equilibrium conditions for the density,  $\rho$ , momentum density  $\mathbf{j}$ , and the momentum flux density  $\mathbf{\Pi}$ :

$$\rho = \sum n_i^{eq} \quad (5)$$

$$\mathbf{j} = \rho \mathbf{u} = \sum \mathbf{c}_i \cdot n_i^{eq} \quad (6)$$

$$\mathbf{\Pi} = \rho(\mathbf{u}\mathbf{u} + c_s^2\mathbf{I}) = \sum n_i^{eq} \cdot \mathbf{c}_i \mathbf{c}_i \quad (7)$$

must also be satisfied. The solvent molecules interact with each other through collisions which dissipate momentum and relax back to equilibrium. The changes in the velocity distributions, as a result of these collisions, arise according to:

$$n_i(\mathbf{r} + \mathbf{c}_i\Delta\tau, t + \Delta\tau) = n_i(\mathbf{r}, t) + \mathbf{L}_{ij} [n_j(\mathbf{r}, t) - n_j^{eq}(\mathbf{r}, t)] \quad (8)$$

where  $\mathbf{L}$  is a collision operator for fluid particles collisions such that the fluid always relaxes back to the equilibrium distribution. For small Knudson and Mach numbers, this

equation has been shown to be equivalent to the Navier-Stokes equation [31]. Our system meets these criteria: the fluid speed is much less than the speed of sound and the mean free path of the fluid, in this case water, is much less than the characteristic length scale of the simulation, the lattice spacing ( $\Delta x = 0.5\mu\text{m}$ ).

The collision operator can be transformed from velocity space into hydrodynamic moment space,  $M_q = \mathbf{m} \cdot \mathbf{n}$ , where  $M_q$  is the  $q^{\text{th}}$  moment of the distribution,  $\mathbf{m}$  is the transformation matrix and  $\mathbf{n} = (n_0, n_1, \dots, n_{18})$ . The density, momentum density, momentum flux, and the kinetic energy flux constitute the nineteen moments. The collision operator,  $\mathbf{L}$ , is chosen to be a diagonal matrix with elements  $\tau_0^{-1}, \tau_1^{-1}, \dots, \tau_{18}^{-1}$ , where  $\tau_q$  is the characteristic relaxation time of the moment  $q$ . The conserved moments, such as density and momentum, have  $\tau^{-1} = 0$ . The other moments, such as the hydrodynamic stress have a single relaxation time,  $\tau_s$  [32]. For these simulations,  $\tau_s = 1.0$ . The focus of this model is how electrostatic interactions and local changes in the fluid momentum affect polyelectrolyte thermophoresis. Thus, the fluid model only conserves fluid density and momentum, and thermal convection of the fluid is neglected.

## B. DNA model

A worm-like chain model is employed for DNA chains [33–35]. The parameters of the model have been selected to match the dynamics of YOYO-stained  $\lambda$ -DNA in bulk solution at 298 K. We model the 48.5kbp  $\lambda$ -DNA with 11 beads connected by 10 springs. The position and velocity of the beads are updated using the explicit Euler method. The forces acting on the bead include excluded volume effects, the elastic force of the springs, the viscous drag force, the electrostatic force, and the Brownian motion of the particles.

The Gaussian excluded volume potential ensures that the DNA behaves according to self-avoiding statistics and is given by:

$$U_{ij}^{ev} = \frac{1}{2} k_B T \nu N_{ks}^2 \left( \frac{3}{4\pi S_s^2} \right) \exp\left( \frac{-3|r_i - r_j|^2}{4S_s^2} \right) \quad (9)$$

where  $\nu = \sigma_k^3$  is the excluded volume parameter with  $\sigma_k = 0.105\mu\text{m}$  (the length of one Kuhn segment),  $N_{ks} = 19.8$  is the number of Kuhn segments per spring and  $S_s^2 = (N_{ks}/6)\sigma_k^2$  is the characteristic size of the bead. The ions and DNA beads interact with each other through entropic excluded volume forces, in addition to electrostatic forces. The parameters for interactions with ions are the same, except for the excluded volume radius. To more accurately capture the ions, the excluded volume radius of the ions is reduced to 1/10 that of a DNA bead, to approximately 20nm. Thus the excluded volume force is reduced by a factor of 10 for ion-bead and a factor of 100 for ion-ion interactions.

The Marko-Siggia [36] force extension relation is used

to calculate the DNA elastic force, given by:

$$\mathbf{f}_{ij}^s = \frac{k_B T}{2\sigma_\kappa} \left[ \left( 1 - \frac{|\mathbf{r}_j - \mathbf{r}_i|}{N_{ks}\sigma_\kappa} \right)^{-2} + 4 \frac{|\mathbf{r}_j - \mathbf{r}_i|}{n_\kappa\sigma_\kappa} - 1 \right] \frac{\mathbf{r}_j - \mathbf{r}_i}{|\mathbf{r}_j - \mathbf{r}_i|} \quad (10)$$

The force extension relation is accurate when  $N_{ks} \gg 1$ . Combined with the bead-bead repulsion, the equilibrium spring length is  $0.5\mu\text{m}$ .

The solvent exerts a frictional viscous drag in the beads given by:

$$\mathbf{F}_f = -\zeta(\mathbf{u}_p - \mathbf{u}_f) \quad (11)$$

where  $\mathbf{u}_p$  is the velocity of the bead and  $\mathbf{u}_f$  is the velocity of the fluid at the bead position, and  $\zeta = 6\pi\eta a$  is the friction coefficient:  $\eta$  is the fluid viscosity and  $a$  is the hydrodynamic radius of the species. The hydrodynamic radius for ions is 1/10 that of the radius of the DNA beads. Thus the ion diffusivity is ten times higher than a DNA bead's diffusivity.

The simulation lattice size,  $\Delta x$ , is chosen to be  $0.5\mu\text{m}$ . For this model, each bead on a DNA chain has a hydrodynamic radius of  $a = 0.077\mu\text{m}$ , or  $0.154\Delta x$  [27]. Since the positions of the beads are not limited to the lattice site where the fluid velocity is well defined, the fluid velocity at the position of the bead is determined by linear interpolation of the velocities of the nearest neighbor (nn) lattice sites such that  $\mathbf{u}_f = \sum_{i \in (nn)} w_i \mathbf{u}_i$ . The weighting factors  $w_i$  are normalized and  $\mathbf{u}_i$  represents the fluid velocity at site  $i$ . The momentum transfer to the bead is  $\Delta \mathbf{j} = -\mathbf{F}_f \Delta t / \Delta x^3$ . The bead will also transfer this momentum to the fluid at a neighboring site  $i$  with velocity  $q$ , such that  $\Delta \mathbf{f}_i = w_i \rho a c_q \Delta \mathbf{j} \cdot \mathbf{c}_q$  [27]. The advantage of the LBM is that the momentum balance and thermal fluctuations of the beads are satisfied locally. In addition, this explicit interaction between the DNA or ion beads and the fluid is necessary to observe thermophoresis. In Brownian dynamics based simulations where hydrodynamic interactions are incorporated through the Oseen-Burger tensor [25], thermophoresis was not observed since a difference in the local fluid stress must develop for the phenomenon to occur [24]. These simulations include hydrodynamic interactions explicitly through the momentum exchange between beads and the surrounding fluid.

The beads undergo Brownian motion according to the local temperature that varies with the bead position. The local equilibrium approximation is invoked to equilibrate the bead and the fluid temperature, while thermal convection of the fluid is neglected. This is the only interaction in which the temperature gradient is taken into account. The thermal fluctuations of the beads are drawn from a Gaussian distribution with zero mean and a variance that depends on the bead position:  $\sigma_\nu = 2k_B T(y)\zeta \Delta t$ . Here,

$$T(y) = \frac{2(T_{hot} - T_{cold})}{Y_{max}} |Y_{max}/2 - y| + T_{cold} \quad (12)$$

where  $Y_{max}$  is the width of the channel, and  $y$  is the position of the bead in the channel.  $T_{hot}$  is the maximum

temperature at the boundaries and  $T_{cold}$  is the minimum temperature in the channel center. This gives a sawtooth shaped temperature profile, a periodic temperature profile is necessary since periodic boundary conditions are imposed in all directions.

The beads of the model DNA interact with dissolved salts and counter-ions through electrostatic interactions. For every one DNA bead that bears a -1 charge, there is one counter-ion with a +1 charge. The dissolved salts occur as pairs, one bearing a +1 charge and the other bearing a -1 charge. Both the counter-ions and the dissolved salts are modeled as point charges. The electrostatic force is calculated using Coulomb's Law:

$$\mathbf{F}_E = k \frac{q_1 q_2}{r^2} \hat{\mathbf{r}} \quad (13)$$

where  $q_1$  and  $q_2$  are charges (either +1 or -1),  $r$  is the distance between them, and  $\hat{\mathbf{r}}$  is the unit vector in the direction of the line connecting the centers of the charges. The constant  $k$  is the electric constant and is the same for both DNA-DNA, DNA-ion, and ion-ion interactions. The electric constant can be varied in simulation to change the strength of the electrostatic interaction and therefore the Debye length. Mathematically, this is equivalent to increasing or decreasing the charge density on the polyelectrolyte or the charge of the dissolved salt since, for example, doubling  $q_1, q_2$ , or  $k$  would result in doubling the force. The parameters  $q_1$  and  $q_2$  can be changed in experiments where  $k$  cannot be varied. The total force on each bead or ion is calculated by summing over all possible pair interactions. A long range cut-off of one half the system size and a short range cut-off of 0.01 lattice spacings is imposed, thus  $0.01\Delta x < r < 10\Delta x$ . The container size and cut-offs were varied, but this did not significantly change  $D_T$  or  $S_T$ .

Despite the simple and coarse-grained nature of the model, it has been shown to quantitatively predict the DNA thermophoretic diffusivity from previous experiments with  $D_T$  for  $\lambda$ -DNA measured as  $0.4\mu m^2/s/K$  [5, 24]. The effect of the coarse-grained model on DNA thermophoresis was examined by varying the degree of DNA coarse-graining. In simulations with no salt molecules added,  $D_T$  was found to not depend on the degree of coarse-graining.

Each of the forces is necessary to model the experimental systems in [5, 6]. The viscous and Brownian forces coupled to a lattice-Boltzmann fluid are required to produce the local gradient in the fluid stress around polymer beads, which causes thermophoresis of neutral polymers [24]. The excluded volume force, spring force, and hydrodynamic interactions are necessary to capture long chain dynamics and to prevent the polymer or salt molecules from becoming too concentrated in any one region. Finally, we will also investigate the role of the salt molecules in thermophoresis.

### C. Simulation Parameters

10  $\lambda$ -DNA chains were simulated in a system of size  $1\mu m \times 10\mu m \times 10\mu m = 2\Delta x \times 20\Delta x \times 20\Delta x$  with periodic boundary conditions in all directions. The concentration of DNA is below the dilute-semi-dilute crossover. The number of salt molecules was varied from 22 to 440. The Debye length is 0.3-1.7 lattice spacings ( $0.15\mu m$ - $0.85\mu m$ ) as calculated according to  $\lambda_D = \sqrt{\frac{k_B T}{2k[salt]}}$  where  $[salt]$  is the concentration of salt molecules and  $k$  is the electric constant from eqn. 15. The temperature profile is a periodic sawtooth function with minimum at  $y = Y_{max}/2$  to allow periodic boundary conditions to be imposed. By matching the model DNA relaxation time at  $T = T_{cold}$  to the  $\lambda$ -DNA relaxation time, the time step for the fluid is  $\Delta\tau = 8.8 \times 10^{-6}s$  (0.05 in simulation units) and for the polymer  $\Delta t = 1.76 \times 10^{-6}s$  (0.01 in simulation units). The total simulation time corresponds to 528 seconds, with data collected once every 1.76 seconds to ensure independent configurations are sampled; the final 200 configurations were averaged to determine  $S_T$  and  $D_T$ . For each set of parameters, 5 different simulations were conducted, each starting from a different random initial configuration.

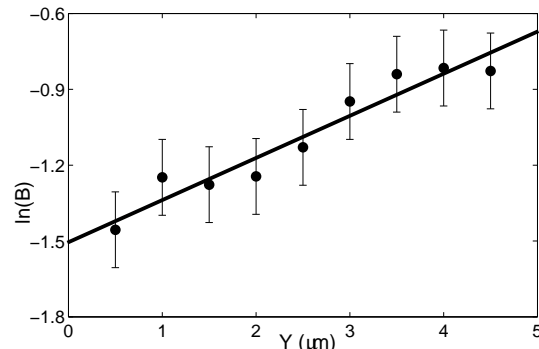


FIG. 1: Log of the concentration of DNA beads in the steady state plotted versus position in channel. The thermal diffusion coefficient is determined from the slope of the linear fit. Here  $D_T = 0.53 \times \mu m^2/s/K$ . Data shown is the average of five independent simulations with 10  $\lambda$ -DNA chains, 220 salt molecules, and  $\Delta T = 2K$  between  $y = 0$  or  $y = Y_{max}$  ( $10\mu m$ ) and  $y = Y_{max}/2$  ( $5\mu m$ ).

## III. RESULTS

The average DNA bead concentration  $\langle B(y) \rangle$  from 5 simulations collected over the last 200 configurations of each trial is shown in figure 1. The bead concentration profile corresponds to the fluorescence intensity profile measured in experiments [5, 6]. It is observed that DNA migrates towards lower temperatures ( $T$  linearly decreases as  $y$  increases). With  $\partial T / \partial y = 0.4K/\mu m$ , one

DNA Length (kbp)	$D_T (\mu\text{m}^2/\text{s}/\text{K})$
67.9	$0.36 \pm 0.1$
48.5	$0.53 \pm 0.09$
19.4	$0.62 \pm 0.06$

TABLE I: Dependence of  $D_T$  on DNA length. The total number of DNA beads (110 beads, or 5, 10, and 20 chains) in the simulation and the number of salt molecules (220 ions, 110 molecules) were the same for each simulation. Error in the measurement was calculated from the standard deviation of concentration measurements from five simulations started with different random initial conditions.

obtains  $B(y) = \exp(0.4S_T y)$  for  $B \ll 1$  from eq. (2)[37]. The slope of  $\log(B(y))$  vs  $y$  yields  $S_T$ , from which  $D_T$  is determined to be  $0.53 \mu\text{m}^2/\text{s}/\text{K}$ . This value is within the range of values reported in experiment for different Debye lengths [5, 6]. When electrostatic interactions and ions are neglected,  $D_T$  was measured to be  $0.4 \mu\text{m}^2/\text{s}/\text{K}$  in both experiment and simulation[5, 24].

Table 1 shows  $D_T$  for different lengths of DNA.  $D_T$  increases as chain length decreases as in some experiments [1, 6]. This length dependence arises due to the inclusion of dissolved salt ions and the electrostatic force. In previous simulations without electrostatics, no length dependence was observed [24]. This is qualitatively the same as the difference between the experiments in [5], which did not show length dependence of  $D_T$ , and [6] which did. Many experiments with neutral polymers have not observed this length dependence [2], our results do not contradict these experiments since the length dependence arises from the electrostatic interaction with dissolved salts.

However, the quantitative dependence of  $D_T$  and  $S_T$  on DNA length in our simulations is different from that in [6]. This may be attributed to the significantly different DNA lengths studied in [6] from the ones modeled

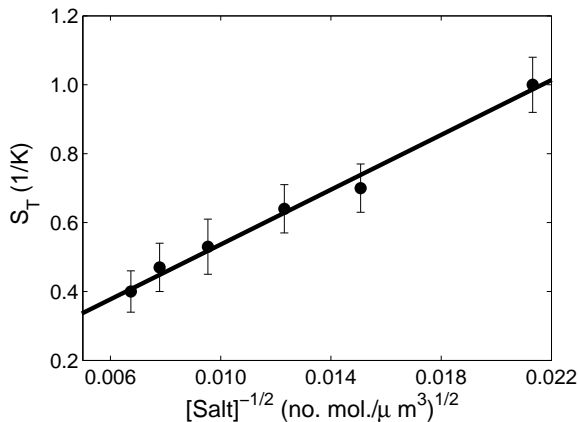


FIG. 2: Dependence of  $S_T$  on  $[\text{salt}]^{-1/2}$ , or Debye length ( $\lambda_D \propto [\text{salt}]^{-1/2}$ ). The line represents a linear fit to the data. The calculation is done with  $\lambda$ -DNA,  $k = 0.0003$  is held constant, and  $\Delta T = 2\text{K}$ .

here. The short DNA in the experimental study is smaller than the dsDNA persistence length and is rod-like. The DNA modeled here is coil-like. In addition, the salt concentration in the simulation is much lower than in the experiments due to the computational constraint on the total number of molecules. Other experiments have also shown a difference in size dependence of  $D_T$  of colloids from the results in [6] due to the complexity of the interactions between particles and solvent [8].

### A. Debye length dependence of $S_T$

Simulations at various salt concentrations were performed to determine the dependence of  $S_T$  on Debye length. Figure 2 shows that  $S_T$  increases as  $\lambda_D$  increases since  $\lambda_D \propto [\text{salt}]^{-1/2}$ . Fig. 2 shows that simulations of polyelectrolytes also exhibit a linear dependence, predicted in [6]. Others have observed or proposed other functional forms for the dependence of  $S_T$  on Debye length for spherical SDS micelles[13]. Our results may differ due to these differences in geometry. In addition, our simulation has only a small number of charges for each polyelectrolyte molecule and a small number of salt molecules due to the computational time necessary to run simulations with more species. This might limit the applicability of our results.

Effects of the electrostatic strength on thermophoresis is further investigated by changing  $k$ , which also changes the Debye length. Fig. 3 shows that as  $k$  increases,  $S_T$  increases as well. It is found that for sufficiently large  $k$ ,  $S_T \propto \sqrt{k}$ . This agrees with the prediction in [5], that  $S_T \propto k * \lambda_D \propto \sqrt{k}$ . For  $k$  smaller than the range plotted in Fig. 3, normal diffusion dominates and fluctuations in bead density are too large to observe a gradient in DNA concentration, suggesting that DNA migration towards the colder region is hindered.

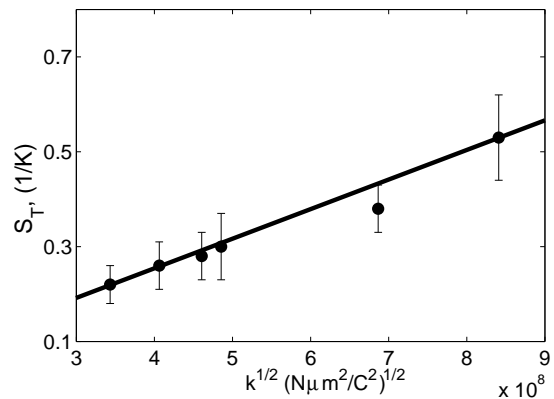


FIG. 3: Dependence of  $S_T$  on electrostatic force. The line represents the linear fit to the data. The calculation is done with  $\lambda$ -DNA, 220 salt ions, and  $\Delta T = 2\text{K}$ .

## B. Mechanism of Thermophoresis

To understand the complex particle dynamics during thermo-migration, the time evolution of the particle concentration profile for DNA and the ions are examined, as shown in Fig. 4. The smaller ions have higher diffusion coefficients than the DNA beads, and they migrate faster to the cold region. As seen in Fig. 4, the ion concentration profile reaches steady state in under 30 seconds, while the DNA bead concentration profile does not reach steady state until after 250 seconds. This indicates that there is a competition between the osmotic pressure due to the non-uniform ion concentration profile that hinders DNA chain migration, and the electrostatically and thermophoretically driven migration of DNA chains towards the colder region.

Fig. 5 shows a non-uniform ion concentration profile and a resulting electric field developed as proposed in [13]. The local charge in a  $xz$ -cross sectional slice of the channel ( $2\Delta x \times 1\Delta x \times 20\Delta x$ ) is shown across the channel. The system is neutral with the same number of positive and negative charges, but the larger DNA, which is negatively charged, migrates in the temperature gradient more slowly than the small positive counterions. A small positive charge on the cold side and a small negative charge accumulation on the hot side develops due to this difference in the Soret coefficients of the charged DNA and dissolved salts. The portion in between the cold and hot regions is effectively neutral. We expect that for a larger channel with a higher concentration of salt molecules, the neutral portion would be larger than in our small system. This charge difference between the hot and the cold regions must affect DNA chain migration. DNA beads will be attracted to the cold side. This acts to enhance thermophoresis. This mechanism is similar to that proposed in [13] for the enhancement of thermal migration of micelles by an induced electric field gener-

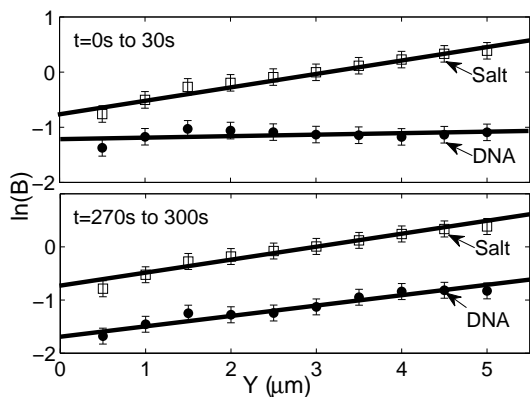


FIG. 4: Density profile of DNA beads(●) and salt molecules(□) averaged over  $t=0s$  to  $t=30s$  (top) and  $t=270s$  to  $t=300s$  (bottom). The best fit line is shown for each plot to show the development of the concentration gradient.

ated by differentially migrating charged species. When the electrostatic strength is weak, this attraction becomes negligible and overcome by the osmotic pressure caused by the non-uniform ion concentration.

Other than electrostatics, the interparticle forces that affect thermodiffusion are the short ranged entropic excluded volume force and the long ranged hydrodynamic interactions, which are repulsive. If the strength of the electrostatic attraction is reduced, then the DNA bead migration is hindered by excluded volume and hydrodynamic forces, as well as the ion osmotic pressure. The DNA thermal diffusion coefficient would then decrease as  $k$  decreases until it reaches 0. In the case with no electrostatic interactions, the steady state is analogous to the size segregation induced by thermophoresis in granular media [38, 39], where the granular particles only repel each other. Of the repulsive forces, the dominance of excluded volume can be inferred from the enhanced thermophoresis in its absence. If both the electrostatic and excluded volume forces are reduced to 0, the thermal diffusion coefficient of  $\lambda$ -DNA is more than doubled, with  $D_T = 1.3\mu m^2/s/K$  for the same conditions as the data plotted in Figure 1.

## IV. CONCLUSION

The results indicate that the mechanism governing thermophoresis is complicated and many factors contribute to polyelectrolyte migration. These include the salt concentration, the thermophoresis of the ions, the charge of the ions, strength of the electrostatic interaction, and the interparticle entropic repulsion. While data shows that a decrease in salt concentration increases  $S_T$ ,

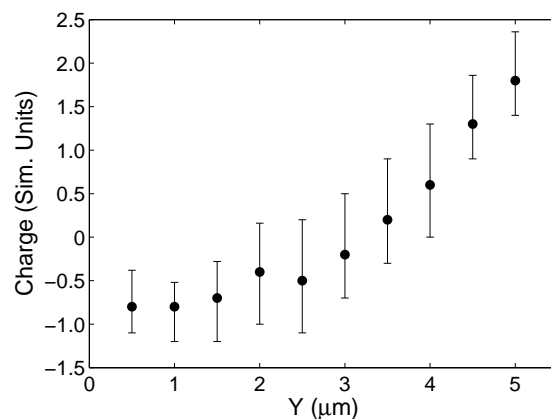


FIG. 5: Net charge in units of  $q$ , the charge of a single DNA bead, in a  $2\Delta x \times 1\Delta x \times 20\Delta x$  ( $1\mu m \times 0.5\mu m \times 10\mu m$ ) slice. For this simulation, 10 DNA molecules with 330 salt molecules are simulated with a 2K temperature difference. The net charge in a region is calculated by summing the charge of all species in a region. Shown is the average over the final 200 time steps.

we also find that when the strength of the electrostatic interaction is decreased, the DNA chains do not migrate. This indicates that the electrostatic interaction and excluded volume repulsion between DNA and dissolved ions are integral in determining  $S_T$ .

What then is the impact of the dissolved ions on the system? It seems as though one explanation cannot fit the entire data set. Similar to studies on miscelle thermophoresis conducted by Vigolo and colleagues [13] and polymer thermophoresis by Stadelmaier and Kohler [3] and Rauch *et al.* [4], we find that there are two regimes of mobility. In [13],  $S_T$  of SDS micelles was found to depend on the thermal migration of an additional electrolyte species. If the migration of the cation and anion of the electrolyte were sufficiently different, an electric field developed in the solution and electrostatic interactions partially determined the migration of the micelles. In this study, we also find the development of an electric field that enhances thermal migration when the electrostatic interaction is strong enough.

In polymer thermophoresis studies [3, 4], it was found that mobility of polymers did not significantly change with a change in polymer concentration in the dilute regime; however, near the glass transition, mobility decreases markedly with increasing concentration, suggesting two regimes. In the dilute regime, the friction the polymers experience is constant throughout the system and the solvent viscosity determines  $D_T$ . In the concentrated regime, the effective local viscosity becomes more important and the environment near the polymer is key.

In our work, when the electrostatic interaction is decreased, forces that are local to a single DNA bead and neighboring salts such as excluded volume repulsion become dominant. The dominance of short-ranged local interactions is also supported by our previous work in which the near field hydrodynamic stress gradient is found to cause thermophoresis of a neutral polymer [24]. However, as  $F_E$  becomes dominant, long range approaches are more appropriate.

The predictions from this study need to be further verified with new experiments to test the effects of increasing electrostatic strength. First, adding multi-valent ions should enhance thermophoresis since increasing  $k$  in eqn. 15 is mathematically equivalent to increasing the charge of the dissolved ions. However, care needs to be taken to prevent DNA molecules from undergoing the coil-globule transition when multivalent salt is added [40]. This study also suggests that by adding a smaller species, such as nanoparticles, to polyelectrolyte solutions, polyelectrolyte thermophoresis may be hindered. In addition, since the simulation is a coarse grained model of DNA, we expect our results are applicable to the experimental studies of other polyelectrolytes as well.

A. Hammack and J.K. Pearce thank H. Neil Gray and A. Randy Back for helpful discussions. They are supported by a grant from the Welch Foundation, number BP-0037 and the University of Texas system Louis Stokes Alliance for Minority Participation, NSF grant number HRD-0703584. Y.L. Chen is supported by the ROC National Science Council (98-2112-M-001-004-MY3).

- 
- [1] S. Iacopini, R. Rusconi, and R. Piazza, Euro. Phys. E. **19**, 59-67 (2006).
- [2] S. Wiegand, J. Phys: Condens. Matter **16**, R357 (2004).
- [3] D. Stadelmaier and W. Köhler, Macromolecules **41**, 6205 (2008).
- [4] J. Rauch, M. Hartung, A. Privalov, and W. Köhler, J. Chem. Phys. **126** (2007).
- [5] S. Duhr, S. Arduini, and D. Braun, Euro. Phys. E **15**, 277 (2004).
- [6] S. Duhr and D. Braun, PNAS **103**, 19678 (2006).
- [7] R. Piazza and A. Guarino, Phys. Rev. Lett. **88**, 208302 (2002).
- [8] M. Braibanti, D. Vigolo, and R. Piazza, Phys. Rev. Lett. **100** (2008).
- [9] S. A. Putnam and D. G. Cahill, Langmuir **21**, 5317 (2005).
- [10] R. Kita, S. Wiegand, and J. Luettmer-Strathmann, J. Chem. Phys. **121**, 3874 (2004).
- [11] S. Iacopini and R. Piazza, Europhys. Lett. **63**, 247 (2003).
- [12] R. Khare, M. D. Graham, and J. J. de Pablo, Phys. Rev. Lett. **96**, 224505 (2006).
- [13] D. Vigolo, S. Buzzaccaro, and R. Piazza, Langmuir (2010).
- [14] J. G. Dhont, S. Wiegand, S. Duhr, and D. Braun, Langmuir **23**, 1674 (2007).
- [15] S. Fayolle, T. Bickel, S. LeBoiteux, and A. Würger, Phys. Rev. Lett. **95**, 208301 (2005).
- [16] E. Ruckenstein, J. Colloid Interface Sci. **83**, 77 (1981).
- [17] S. N. Semenov and M. Schimpf, Phys. Rev. E **69**, 011201 (2004).
- [18] K. Morozov, in *Thermal Nonequilibrium Phenomena in Fluid Mixtures*, edited by S. Wiegand and W. Köhler (Springer, Berlin, 1999), p. 38.
- [19] K. Morozov, JETP **88**, 944 (1999).
- [20] A. Parola and R. Piazza, Eur. Phys. J. E **15**, 255 (2004).
- [21] A. Würger, Phys. Rev. Lett. **98**, 138301 (2007).
- [22] A. Würger, Phys. Rev. Lett. **101**, 108302 (2008).
- [23] H. Ning, J. Dhont, and S. Wiegand, Langmuir **24**, 2426 (2008).
- [24] J. Kreft and Y.-L. Chen, Phys. Rev. E **95**, 021912 (2007).
- [25] Y.-L. Chen, H. Ma, M. D. Graham, and J. J. dePablo, Macromolecules **40**, 5978 (2007).
- [26] P. Ahlrichs and B. Dünweg, J. Chem. Phys. **111**, 8225 (1999).
- [27] P. Ahlrichs and B. Dünweg, Int. J. Mod. Phys. **9**, 1429 (1998).
- [28] A. J. C. Ladd, J. Fluid Mech. **271**, 285 (1994).
- [29] O. Berk Usta, A. J. C. Ladd, and J. E. Butler, J. Chem. Phys. **122**, 094902 (2005).
- [30] O. Berk Usta, J. E. Butler, and A. J. C. Ladd, Phys. Fluids **18**, 031703 (2006).
- [31] R. Benzi, S. Succi, and M. Vergassola, Phys. Rep. **222**, 145 (1992).
- [32] P. Bhatnagar, E. P. Gross, and M. K. Krook, Phys. Rev.

- 94**, 511 (1954).
- [33] R. M. Jendrejack, E. T. Dimalanta, D. C. Schwartz, M. D. Graham, and J. J. de Pablo, *Phys. Rev. Lett* **91**, 038102 (2003).
- [34] R. M. Jendrejack, D. C. Schwartz, M. D. Graham, and J. J. de Pablo, *J. Chem. Phys.* **119**, 1165 (2003).
- [35] R. M. Jendrejack, E. T. Dimalanta, D. C. Schwartz, M. D. Graham, and J. J. de Pablo, *J. Chem. Phys.* **116**, 7752 (2002).
- [36] J. Marko and E. Siggia, *Macromolecules* **28**, 8759 (1995).
- [37] S. Duhr and D. Braun, *Phys. Rev. Lett.* **96**, 168301 (2006).
- [38] S. Hsiau and M. Hunt, *Acta Mech.* **114**, 121 (1996).
- [39] M. Schröter, S. Ulrich, J. Kreft, J. B. Swift, and H. L. Swinney, *Phys. Rev. E* **74**, 011307 (2006).
- [40] V. A. Bloomfield, *Curr. Op. Struct. Biol.* **74**, 334:341 (1996).